Magnetic and electronic properties of ternary uranium antimonides $UTSb_2$ ($T=3d$-, $4d$-, $5d$-electron transition metal)

D. Kaczorowski*
W. Trzebiatowski Institute for Low Temperature and Structure Research, Polish Academy of Sciences, P.O. Box 937, 50-950 Wrocław 2, Poland

R. Kruk† and J. P. Sanchez
Département de Recherche Fondamentale sur la Matiere Condensée, CEA/Grenoble, 17 rue des Martyrs, 38054 Grenoble Cedex 9, France

B. Malaman
Laboratoire de Chimie du Solide Minéral associé au CNRS (URA 158), Université Henri Poincaré-Nancy I, B.P. 239, 54506 Vandoeuvre les Nancy Cedex, France

F. Wastin
European Commission, Joint Research Center, Institute for Transuranium Elements, Postfach 2340, D-76125 Karlsruhe, Germany
(Received 17 March 1998)

Magnetic, electrical transport, neutron diffraction, and Mössbauer measurements have been performed on a series of uranium–transition-metal–antimonides $UTSb_2$ (T=Fe, Co, Ni, Cu, Ru, Pd, Ag, and Au). Most of these compounds were found to order magnetically at low temperatures and characterized as semimetallic Kondo lattices with strongly screened magnetic moments. Combined neutron diffraction and Mössbauer results allowed determination of the magnetic structures adopted in antiferromagnetic $UNiSb_2$, $UPdSb_2$, and $URuSb_2$. The magnetic behavior found in $UTSb_2$ phases is here discussed with a special emphasis on the role of the f-p and f-d hybridization. [S0163-1829(98)00538-4]

I. INTRODUCTION

Uranium compounds UTX_2, where T is a $3d$-, $4d$-, or $5d$ transition metal and X stands for a pnictogen, form a numerous family of ternaries, closely related to the well-known UX_2 phases. Most of them crystallize in a simple tetragonal structure (space group $P4/nmm$, see Fig. 1) usually referred to in the literature as $ZrCuSi_2$, $HfCuSi_2$, $UCuAs_2$, or ZrCuSiAs type. Although $UCuAs_2$ was the first pnictide reported to form with this structure,[1] the very first compound for which the corresponding atomic positions have been determined was $HfCuSi_2$.[2] For this reason, accepting the arguments presented recently by the authors of Ref. 3, the prototype name $HfCuSi_2$ will be consequently used in this and our further papers on UTX_2 pnictides.

Previously, in a series of publications we reported on the magnetic, transport, and thermal properties of several 1:1:2 uranium–transition-metal phosphides and arsenides (Ref. 4, and references cited therein). There, we addressed mainly the problem of how the crystal-field potential acting on the uranium atom and the exchange interactions between them are modified when atoms of a given transition metal are embedded into the unit cell of the respective UX_2 parent compound. Moreover, particular attention was paid to the role of the hybridization between the uranium $5f$ states and the transition-metal d-conduction states and the pnictogen p-valence states in determining the behavior of these phases. In the following we extend our discussion to the uranium antimonides $UTSb_2$. We report here on the preparation of several such compounds and present the results of bulk magnetic, electrical transport, neutron diffraction, and Mössbauer investigations, performed on polycrystalline samples of these materials.

II. EXPERIMENT

Polycrystalline samples of $UTSb_2$ were prepared by arc melting the constituent elements in a purified argon atmo-

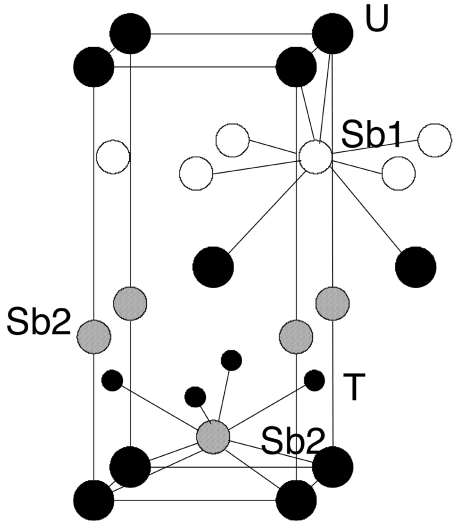

FIG. 1. Crystal structure of $UTSb_2$ compounds. The near-neighbor environment of the Sb1 and Sb2 atoms is outlined.

TABLE I. Lattice parameters for $UTSb_2$ compounds.

Compound	Lattice parameters	
	a (Å)	c (Å)
$UFeSb_2$	4.332(1)	9.320(3)
$URuSb_2$	4.342(2)	9.249(2)
$UCoSb_2$	4.311(2)	9.075(4)
$UNiSb_2$	4.322(1)	9.081(1)
$UPdSb_2$	4.332(1)	9.520(2)
$UCuSb_2$	4.297(1)	9.643(2)
$UAgSb_2$	4.322(2)	10.281(1)
$UAuSb_2$	4.342(1)	9.795(1)

sphere. Some weight losses due to evaporation of antimony were compensated beforehand by correcting the starting compositions by excess amounts of antimony. The buttons were subsequently wrapped in molybdenum foil and annealed in evacuated quartz tubes at 800 °C for two weeks. After the heat treatment the samples were quenched by submerging the tubes in water.

The x-ray powder diffraction examinations were performed on a DRON 1.5 diffractometer with Cu $K\alpha$ radiation. They revealed that the attempts to synthesize $UTSb_2$ compounds with the $HfCuSi_2$-type structure have failed for T=Rh, Ir, and Pt but they have been successful with T =Fe, Co, Ni, Cu, Ru, Pd, Ag, and Au. The tetragonal lattice parameters for these latter eight phases, determined by least-squares refinement, are given in Table I. It is worthwhile noting that the lattice parameters derived for $UAgSb_2$ are rather close to those given in the literature.[3]

Magnetic susceptibility measurements were carried out in the temperature range 4.2–300 K using a Cahn electrobalance. The magnetization was measured in external fields up to 4 T employing a moving sample magnetometer. Electrical resistivity studies were performed over the temperature interval 4.2–300 K using a conventional four-point dc technique.

^{121}Sb Mössbauer measurements (5/2–7/2, 37.2 keV) of $UTSb_2$ (T=Cu, Ni, Pd, and Ru) as well as USb_2 samples were performed using a 660 μCi $Ca^{121m}SnO_3$ source kept either at 4.2 K or 77 K and the absorber at variable temperature from 4.2 to 210 K. The absorber thickness was about 12 mg Sb/cm^2. The spectra were recorded on a sinusoidal drive using conventional methods. The data were directly fitted to the hyperfine parameters by constraining the relative absorption energies and intensities of the Lorentzian lines to theoretical values.

Neutron experiments on polycrystalline $UPdSb_2$ and $URuSb_2$ were carried out at the Institute Laue Langevin, Grenoble. Several diffraction patterns have been recorded in the temperature range 2–300 K (namely, above and below the ordering temperatures) with the one-dimensional curved multidetector D1b (λ=2.524 Å). The first refinements, carried out in the paramagnetic state, indicated the occurrence of strong texture effects (because of the disklike crystallites, the c axis takes a preferential orientation perpendicular to the neutron beam). In order to correct for these texture effects, a procedure largely described in Ref. 5 was applied, and in the final refinements a fitted coefficient, f_{cor}, was used that takes into account the importance of preferential orientation. The

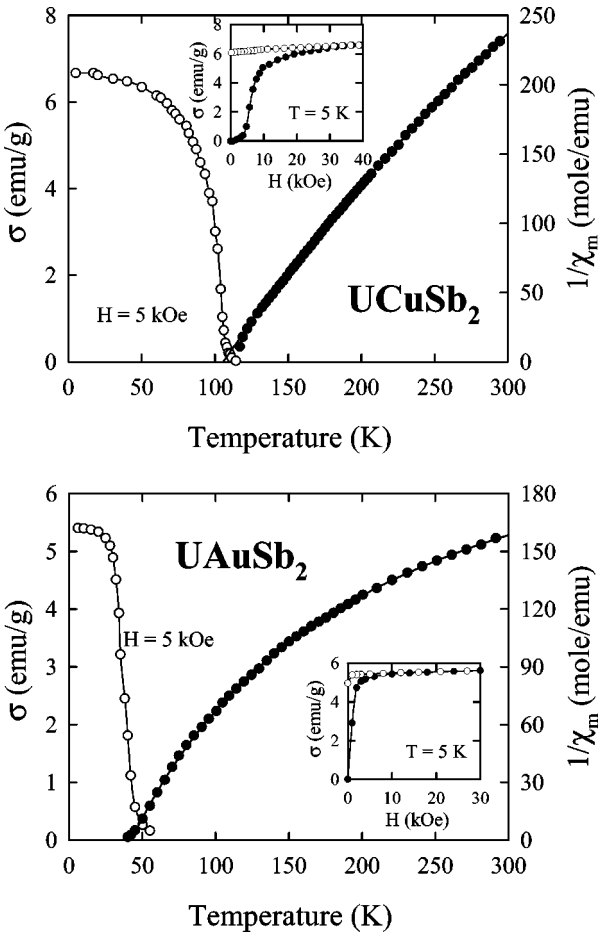

FIG. 2. Temperature dependences of the magnetization (left-hand scale) and the inverse molar magnetic susceptibility (right-hand scale) for the ferromagnets $UCuSb_2$ and $UAuSb_2$. The solid lines are the fits of $\chi^{-1}(T)$ to the modified Curie-Weiss law with the parameters listed in Table II. The insets present the field dependences of the magnetization measured at 5 K with increasing (closed circles) and decreasing (open circles) magnetic field.

form factor of U^{4+} was taken from Ref. 6 and the scattering lengths used in the calculations were as follows: b_U =0.8417 fm, b_{Ru}=0.703 fm, b_{Pd}=0.591 fm, and b_{Sb} =0.551 fm. The least-squares fittings were performed employing the MiXeD crystallographic executive for diffraction.[7]

III. RESULTS AND DISCUSSION

A. Bulk magnetic properties

The results of the susceptibility and magnetization measurements are presented in Figs. 2 and 3. It appears that $UCuSb_2$ and $UAuSb_2$ are strongly anisotropic ferromagnets with the Curie temperatures of 114 and 36 K, respectively, whereas $URuSb_2$, $UNiSb_2$, and $UPdSb_2$ order antiferromagnetically below T_N=127, 175, and 196 K, respectively. A strong tail in $\chi(T)$ observed for $URuSb_2$ at low temperatures may suggest a complex antiferromagnetic structure with some canting of the magnetic moments but it may also be due to some strongly paramagnetic impurities in amount below the detection limit of x-ray powder diffraction. The com-

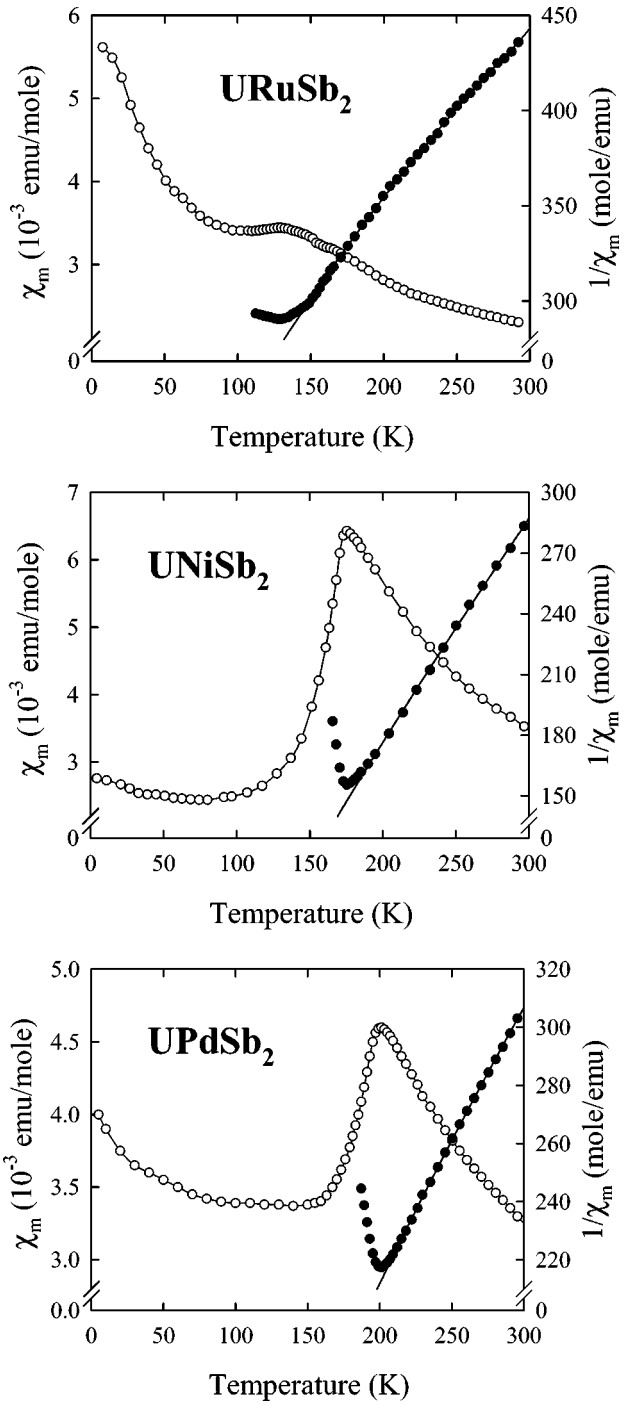

FIG. 3. Temperature dependences of the molar magnetic susceptibility (left-hand scale) and the inverse molar susceptibility (right-hand scale) for the antiferromagnets: $URuSb_2$, $UNiSb_2$, and $UPdSb_2$. The solid lines are the fits of $\chi^{-1}(T)$ to the modified Curie-Weiss law with the parameters listed in Table II.

pound $UAgSb_2$ is probably a ferromagnet with $T_C = 92$ K but evaluation of the magnetic results obtained for this antimonide was hampered by the presence of a small amount of U_3Sb_4 (not seen on the x-ray pattern) which is also ferromagnetic below 146 K. Similarly, in the case of $UFeSb_2$ and $UCoSb_2$, the magnetic behavior could not be determined because of some traces of metallic iron and cobalt present in the samples.

As shown in the insets to Fig. 2, the $\sigma(B)$ curves obtained for $UCuSb_2$ and $UAuSb_2$ saturate in high magnetic fields reaching the magnetic moment of about $1.3\mu_B$ (estimated with the assumption of a uniaxial magnetic anisotropy). In the paramagnetic region the magnetic susceptibility of all the compounds examined follows a modified Curie-Weiss law. The values of the effective magnetic moment μ_{eff}, the paramagnetic Curie temperature θ_p, and the temperature independent term χ_0, derived by least-squares fitting, are given in Table II. It is worthwhile noting that, except for $URuSb_2$, θ_p is always positive which may reflect strong ferromagnetic exchange interaction between the magnetic moments, occurring also in antiferromagnetic $UNiSb_2$ and $UPdSb_2$. This observation is in line with the expected magnetic structures in these compounds, consisting of alternating layers of strongly ferromagnetically coupled uranium magnetic moments.[8] Like the saturation magnetic moments found for ferromagnets, the values of μ_{eff} are always much smaller than the free U^{4+} or U^{3+} ion values. As for many other uranium compounds, this reduction results predominantly from strong crystal-field interactions but in view of our electrical resistivity results (see below) it seems likely that also Kondo-like screening effects may play some role in the overall reduction of the magnetic moment.

B. Electrical resistivity

Figure 4 displays the temperature variations of the electrical resistivity for ferromagnetic $UCuSb_2$, $UAgSb_2$, and $UAuSb_2$. The $\rho(T)$ dependencies for antiferromagnets $URuSb_2$ and $UPdSb_2$ are shown in Fig. 5. In turn, Fig. 6 presents the resistivity of $UFeSb_2$. The shapes of all these curves as well as the absolute values of the resistivity indicate a semimetallic character of the antimonides studied. In all cases the magnetic phase transitions manifest themselves as pronounced anomalies on $\rho(T)$ and sharp extrema in the $d\rho/dT$ vs T functions. It is worth noting that a ferromagnetic-type anomaly is observed also for $UFeSb_2$, which may suggest that this compound is a ferromagnet with T_c of about 30 K. In the paramagnetic region the resistivity always decreases monotonically with increasing temperature in a manner characteristic of Kondo systems.

The behavior of the resistivity was analyzed assuming the validity of the Matthiessen rule. At low temperatures the $\rho(T)$ variations of $URuSb_2$, $UPdSb_2$, $UAgSb_2$, and $UAuSb_2$ can be fairly well fitted by the equation

$$\rho(T) = \rho_0 + aT^2 \exp\left(-\frac{\Delta}{T}\right), \tag{1}$$

where ρ_0 is the residual resistivity and the second term describes scattering of the conduction electrons on spin-wave excitations with the energy gap Δ in the spin-wave spectrum. Only for $UCuSb_2$ and $UFeSb_2$ could no region of a $T^2\exp(-\Delta/T)$ dependence be detected.

In turn, in the paramagnetic region the resistivity of $UPdSb_2$, $UCuSb_2$, $UAgSb_2$, and $UAuSb_2$ follows the standard Kondo formula

$$\rho(T) = \rho_0 + \rho_0^{\infty} - c_K \ln T, \tag{2}$$

where ρ_0^{∞} stands for the spin-disorder resistivity and c_K is the Kondo coefficient. The parameters occurring in the above

TABLE II. Magnetic data for $UTSb_2$ compounds as deduced from magnetization measurements. All the symbols have their usual meaning (see also the text).

Compound	$T_{C,N}$ (K)	μ_0 (μ_B)	μ_{eff} (μ_B)	θ_p (K)	χ_0 (10^{-4} emu/mole)
$UFeSb_2$	P (?)				
$URuSb_2$	AF127(5)		1.91(5)	−40(4)	9.2(7)
$UCoSb_2$	(?)				
$UNiSb_2$	AF175(1)		2.46(3)	57(2)	3.6(9)
$UPdSb_2$	AF196(2)		2.43(2)	20(1)	6.3(6)
$UCuSb_2$	F114(2)	1.3(1)	2.31(2)	105(1)	7.9(7)
$UAgSb_2$	F92(5) (?)				
$UAuSb_2$	F36(3)	1.4(1)	2.25(4)	42(3)	38.5(5)

two functions, found by least-squares fitting procedure, are listed in Table III. It is worth noting that the values of c_K are rather large, which suggests a considerable density of states at the Fermi level in all these intermetallics. The resistivity of $URuSb_2$ and $UFeSb_2$ also decreases strongly with rising temperature over a wide temperature range but no logarithmic variation of $\rho(T)$ was observed for both these compounds.

C. Mössbauer spectroscopy

The Mössbauer spectra of ^{121}Sb in $UTSb_2$ (T=Cu, Ni, Pd, and Ru) obtained at 4.2 K (ordered state) and in the paramagnetic state are reported in Fig. 7. The spectra could be well fitted with two sites by constraining the relative intensities due to the Sb1 and Sb2 atoms in the proportion 1:1 that corresponds to the ratio of the multiplicities of the Sb1 ($2a$) and Sb2 ($2c$) crystallographic sites (see Fig. 1). In the paramagnetic state, the spectra consist of an asymmetric absorption line enlarged by the quadrupolar interactions experienced by the Sb1 and Sb2 atoms. In the ordered state, at 4.2 K, magnetic splittings are clearly seen. However, due to the large natural linewidth of the ^{121}Sb resonance and relatively small hyperfine fields transferred to the Sb atoms, the lines of the spectra are poorly resolved. The results of the data analysis, given in Table IV, indicate that the two types of Sb atoms experience quite different hyperfine interaction parameters. This is not unexpected since the Sb1 and Sb2 atoms occupy sites with entirely different coordinations. The Sb1 atoms have four U neighbors forming a stretched tetrahedron and four Sb1 neighbors forming a square. In turn, the Sb2 atoms are coordinated by four T atoms and four U atoms all in a distorted square antiprism arrangement (see Fig. 1). The assignment of the two sets of hyperfine parameters to their respective Sb1 and Sb2 sites was made following the arguments by Brylak, Möller, and Jeitschko.[3] The formal charge state of the Sb2 atoms is expected to be more negative than that of the Sb1 atoms, since the antimony atoms are the most electronegative component in the $UTSb_2$ compounds and since the Sb2 atoms do not form any Sb-Sb bonds. These considerations allow us to assign the set of hyperfine parameters with the larger (i.e., less negative) isomer shift to the Sb2 atoms ($\Delta\langle r^2\rangle$, the change of the mean square nuclear charge radius, for the ^{121}Sb resonance is negative). This assignment fully agrees with the ^{121}Sb isomer shift systematics, e.g., $\delta_{\text{IS}}=-11.7$, -8.75 and -8.22 mm/s vs $CaSnO_3$ for elemental Sb, NiSb, and USb, respectively.[9,10]

The magnetic fields acting on the nuclei of the Sb atoms are the result of a finite spin density at the Sb sites produced by the uranium magnetic moments through magnetic exchange, either by the polarization of the conduction electrons via the Ruderman-Kittel-Kasuya-Yosida (RKKY) interaction or by covalent mixing of the U5f electrons with the Sb p states. In order to observe a transferred hyperfine field, the uranium moments should be arranged in such a way that their vectorial sum $\Sigma_i\overline{\mu_i}$ in the immediate vicinity of an Sb atom does not vanish. Furthermore, if one assumes that the transferred field is isotropic, its direction with respect to the principal axis of the electrical field gradient tensor (the fourfold tetragonal c axis) provides the orientation of the uranium magnetic moments for collinear magnetic structures. Since the effective quadrupole couplings for both Sb1 and Sb2 atoms are basically the same in the ordered and paramagnetic states, we conclude that the uranium moments point along the tetragonal c axis in all the investigated compounds. Further information on the spin arrangement in the three antiferromagnets, $UNiSb_2$, $UPdSb_2$, and $URuSb_2$, is provided by the transferred hyperfine field at the Sb1 atoms whose uranium neighbors (2 + 2) belong to two successive uranium atom planes, stacked along the c axis (see Fig. 1). The observation of a transferred field indicates a $++$ sequence of uranium atom layers, whereas its absence means that the sequence should be $+-$. Therefore, from the results listed in Table IV, one concludes to a $+--+$ arrangement for both $UNiSb_2$ and $UPdSb_2$ [model (c) in Fig. 8], whereas two structure models, $+-+-$ [model (a) in Fig. 8] and $--++$ [model (b) in Fig. 8], are compatible with the data set of $URuSb_2$.

As concerns the magnitude of the transferred hyperfine fields at the Sb1 and Sb2 atoms, one should first note that $H_{\text{hf}}^{(1)}$ and $H_{\text{hf}}^{(2)}$ have different values although $\Sigma_i\overline{\mu_i}=4$ for both types of atoms in $UCuSb_2$, $UNiSb_2$, $UPdSb_2$, and USb_2.[11] Actually, Table IV shows that $H_{\text{hf}}^{(1)}<H_{\text{hf}}^{(2)}$ in $UTSb_2$ compounds while the opposite trend is observed in the related USb_2 phase (both structures only differ by the intercalation of a T atom layer). To explain the different H_{hf} values in USb_2 one could invoke the different Sb-U bonding lengths [$d_{\text{Sb1-U}}=3.248$ Å and $d_{\text{Sb2-U}}=3.111$ Å (Ref. 11)]. Yet, such an explanation does not hold for the $UTSb_2$ compounds. Indeed, the Sb1-U bonds are here still weaker than Sb2-U bonds but $H_{\text{hf}}^{(2)}$ is now larger than $H_{\text{hf}}^{(1)}$. This fact clearly emphasizes the importance of the four neighboring T

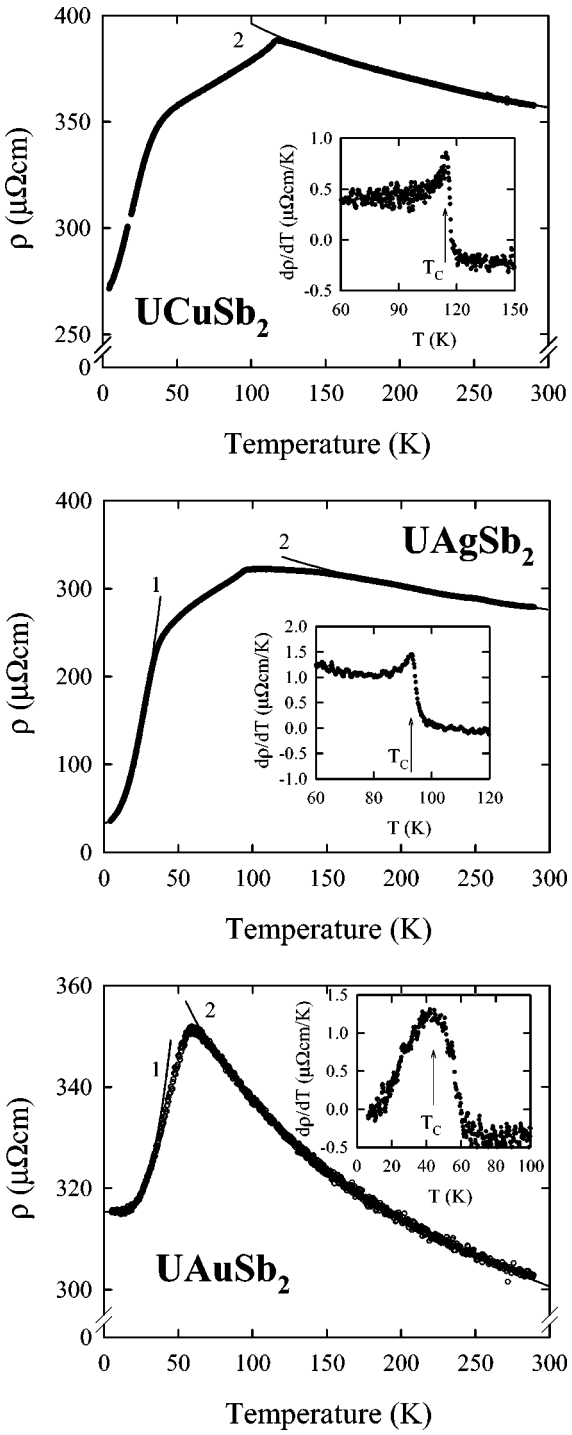

FIG. 4. Temperature variations of the electrical resistivity of ferromagnetic compounds: $UCuSb_2$, $UAgSb_2$, and $UAuSb_2$. The thin solid lines are fits of $\rho(T)$ to Eqs. (1) and (2) (see text). The insets show the temperature derivative of the resistivity in the vicinity of the Curie temperature.

atoms showing up in the first coordination shell of the Sb2 atoms. The intercalation of T atoms into the unit cell of USb_2 provides two additional s-conduction electrons per formula unit. This effect as well as the Sb-T bonding features change dramatically the electronic structure of the Sb2 atoms as shown by the trend of the isomer shifts (see Table IV). Hence, at this stage, i.e., without a detailed knowledge of the

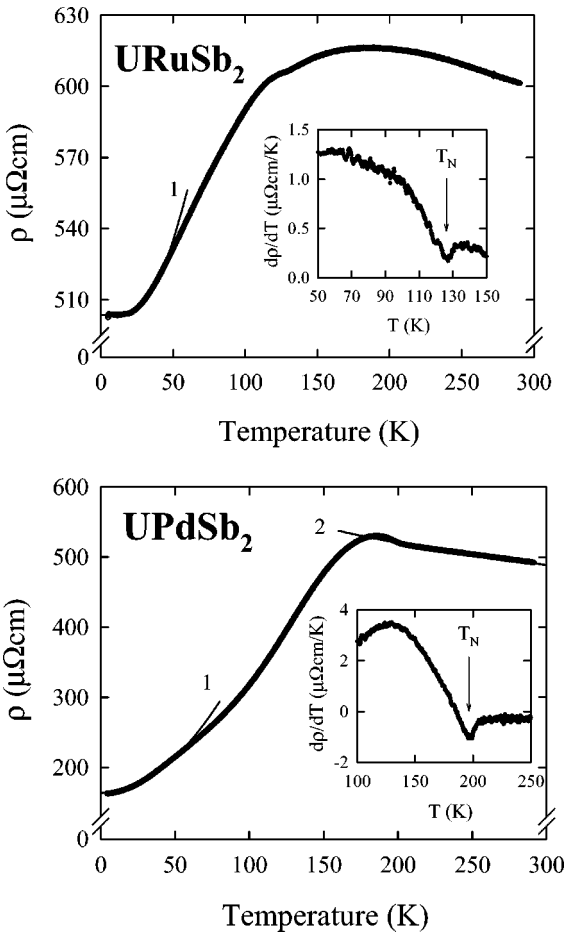

FIG. 5. Temperature variations of the electrical resistivity of antiferromagnetic compounds: $URuSb_2$ and $UPdSb_2$. The thin solid lines are fits of $\rho(T)$ to Eqs. (1) and (2) (see text). The insets show the temperature derivative of the resistivity in the vicinity of the Néel temperature.

electronic structures and of the exchange mechanisms involved, it is not possible to establish any relationship between the magnitude of the transferred hyperfine fields and the magnetic moment carried by the uranium atoms.

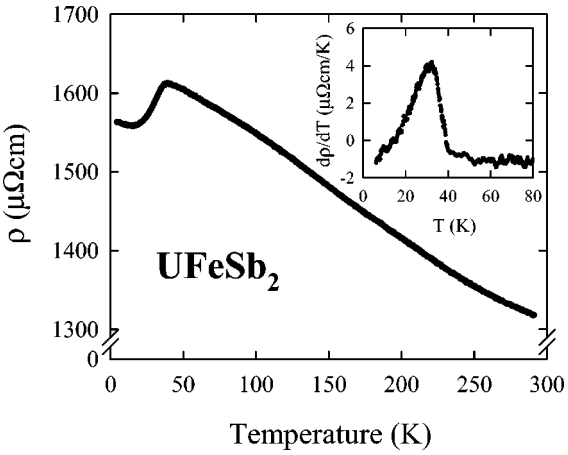

FIG. 6. Temperature dependence of the electrical resistivity of $UFeSb_2$. The inset presents the temperature derivative of the resistivity at low temperatures.

TABLE III. Electrical resistivity data for $UTSb_2$ compounds. For explanation see the text.

Compound	Eq. (1)			Eq. (2)	
	ρ_0 ($\mu\Omega$ cm)	a ($\mu\Omega$ cm/K^2)	Δ (K)	$\rho_0+\rho_0^{\infty}$ ($\mu\Omega$ cm)	c_K ($\mu\Omega$ cm)
$URuSb_2$	503(3)	0.03(2)	46(2)		
$UPdSb_2$	164(4)	0.02(1)	0	931(6)	77.5(8)
$UCuSb_2$				562(4)	35.9(7)
$UAgSb_2$	33(1)	0.19(3)	0	650(3)	65.6(9)
$UAuSb_2$	315(2)	0.07(2)	61(2)	489(5)	33.1(7)

D. Neutron diffraction

The neutron diffraction patterns, collected for $UPdSb_2$ and $URuSb_2$ in the paramagnetic state (see the lower diffractograms in Fig. 9), are characteristic of the space group $P4/nmm$ and confirm the $HfCuSi_2$-type structure for both compounds. Comparison between the observed and calculated intensities of the nuclear peaks is given in Tables V and VI, where also the main results of crystal structure refinements (the lattice parameters, the z_U and z_{Sb2} atomic positions, the March factor f_{cor}, and the reliability factor R) are collected. It is worthwhile noting that a large f_{cor} factor (≈ 1.2) was derived for both compounds which indicates strong texture effects and thus supports the validity of the correction applied.

As is apparent from Fig. 9, the neutron diffraction pattern of $UPdSb_2$, recorded in the ordered state, shows several superlattice Bragg reflections of magnetic origin. The observed magnetic peaks follow the rule $l=(2n+1)/2$, where $n=1, 2, 3, \ldots$. This leads unambiguously to the conclusion that the magnetic unit cell is tetragonal and doubled along the c direction with respect to the chemical unit cell. Moreover, the absence of the magnetic (00l) reflection proves that the magnetic moment is aligned along the fourfold axis. Analysis of the observed magnetic intensities yields two possible sequences of ferromagnetically coupled uranium atom layers: $++--$ and $+--+$, as shown in Figs. 8(b) and 8(c), respectively. A simple criterion discerning these two types of magnetic structure was proposed by Przystawa[12] on the basis of magnetic symmetry considerations. According to this rule, the exchange integral for coupling between the nearest uranium atom layers is negative (i.e., the structure is $+--+$) if the positional parameter $z_U>0.25$, and positive (i.e., the structure is $++--$) if $z_U<0.25$. It is worth noting that Przystawa's criterion works well for known uranium compounds crystallizing with the $P4/nmm$ space group, such as UX_2 pnictides with X = P, As, Sb (the magnetic structure $+--+$) or UOY oxychalcogenides with $Y=$S and Se (the magnetic structure $++--$).[8] In particular, the above rule is followed in the case of $UPdAs_2$ (the compound closely related to the antimonides studied in this paper) for which $z_U<0.25$ and the sequence $++--$ was found.[13] Unfortunately, for $UPdSb_2$ the parameter z_U is very close to the critical value ($z_U=0.252$), and therefore it is not possible to choose unambiguously between the two magnetic structure types, though the solution $+--+$ is slightly marked out. Interestingly, as discussed above, the Mössbauer spectroscopy results have yielded for $UPdSb_2$ just that latter magnetic structure and thus Przystawa's rule seems to be appropriate also in this case. Comparison of the observed and calculated nuclear and magnetic intensities, measured at 2 K, together with the refined values of the lattice parameters and some other adjustable parameters are given in Table V.

The neutron diffraction pattern of $URuSb_2$ taken in the ordered state is presented in Fig. 9. It reveals the appearance of only one additional reflection, namely, (100), which is forbidden by the crystallographic space group. All the magnetic Bragg peaks are indexable within the chemical unit cell and obey the rule $h+k+l=2n+1$, where $n=1, 2, 3, \ldots$. Thus the magnetic unit cell of this compound consists of ferromagnetic (001) sheets of uranium magnetic moments which are arranged antiferromagnetically along the tetragonal c direction according to the sequence $+-+-$. As for $UPdSb_2$, the absence of any magnetic contribution to the (00l) reflection proves that the magnetic moments point along the c axis. It is worth noting that such a magnetic structure, displayed in Fig. 8(a), has previously been found for $UNiAs_2$ (Ref. 14) which is also a representative of the $HfCuSi_2$-type uranium pnictides. Table VI lists the observed and calculated neutron diffraction intensities at 2 K, and gives the refined values of the structural parameters.

Figure 10 shows the thermal variation of the magnetic moment in both $UPdSb_2$ and $URuSb_2$. At 2 K, the ordered moment amounts to $2.2(1)\mu_B$ and $1.2(1)\mu_B$ for the palladium- and ruthenium-based compound, respectively. The extrapolated values of T_N are 225(5) and 135(5) K, respectively, being in good agreement with the bulk magnetic measurements.

IV. HYBRIDIZATION EFFECTS

A crucial point in the discussion of the magnetic properties of UTX_2 pnictides is a question concerning the mechanism of salient change in the character of coupling between adjacent layers of uranium atoms upon incorporating into the unit cell of a given UX_2 compound an extra layer of transition-metal atoms. This question has already been briefly raised in Ref. 4. There, it was argued that the mechanism responsible for the magnetic ordering in UTX_2 phases is probably an interplay of superexchange via metalloid ions and RKKY interaction via conduction electrons. It is expected that an incorporation of T atoms changes the strength of the latter interaction because it causes not only an increase of the U-U distances (mainly along the c axis) but also changes the number of conduction electrons. Obviously, these two effects may explain different magnetic behavior of UTX_2 pnictides with respect to their parent UX_2 compounds. However, it is hardly understandable why the UTX_2 phases with a given X show such a large variety of magnetic prop-

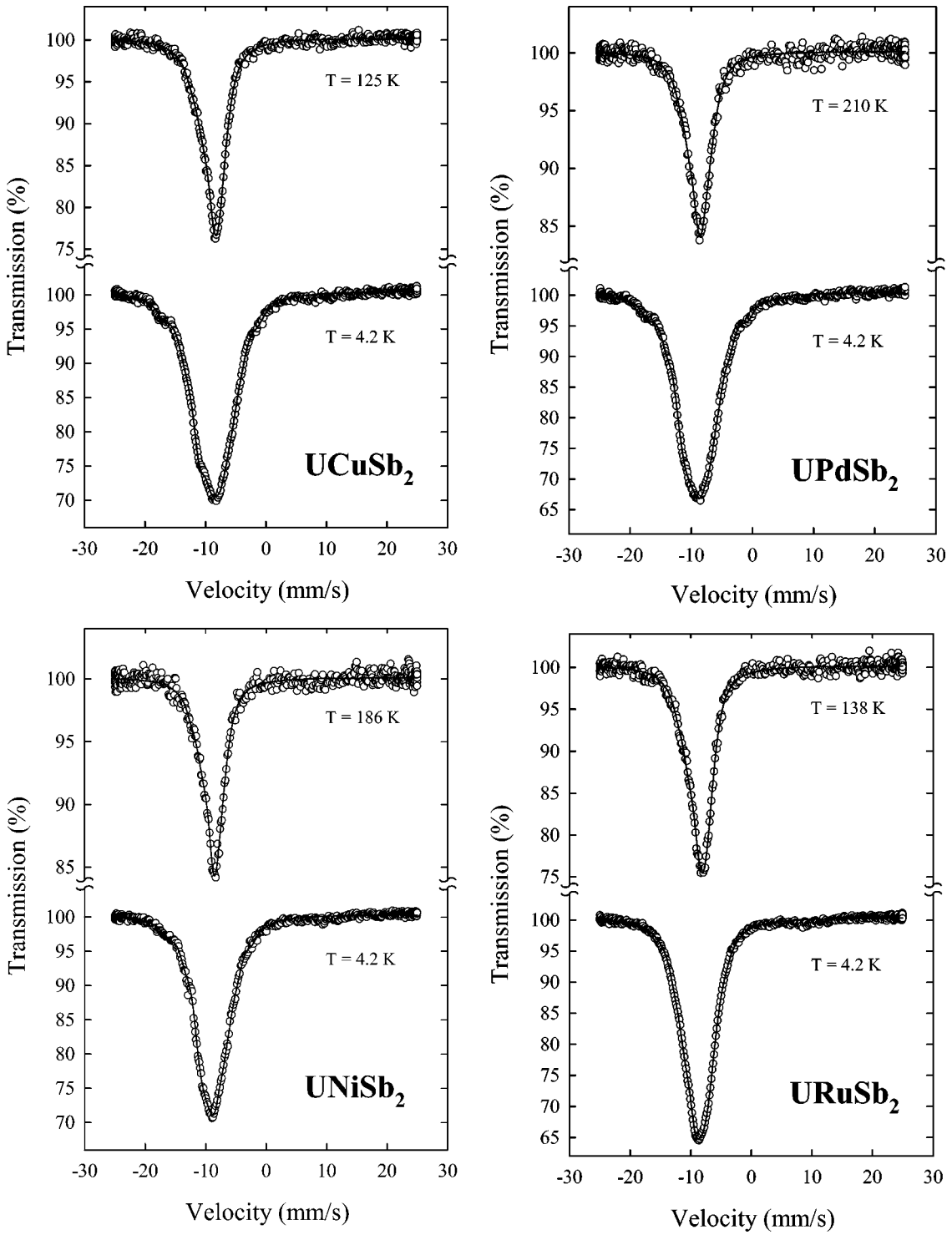

FIG. 7. ^{121}Sb Mössbauer spectra of $UCuSb_2$ at 125 and 4.2 K, $UNiSb_2$ at 186 and 4.2 K, $UPdSb_2$ at 210 and 4.2 K, $URuSb_2$ at 138 and 4.2 K.

erties. For example, in the $UTAs_2$ series, $UCoAs_2$ is ferromagnetic and $UNiAs_2$ is antiferromagnetic despite the closeness of the atomic radii of Co and Ni, and despite the fact that both transition metals introduce two s electrons into the conduction band. Therefore it seems likely that an important role in the magnetism of UTX_2 compounds is played by d electrons of transition metals and that the magnetic behavior of these phases is governed by the interaction of these electrons with $5f$ electrons of uranium.

It is well known that the so-called f-p,d hybridization is the driving mechanism of delocalization of f electrons in many cerium and uranium intermetallics (see, for example, Ref. 15) being in this manner the main factor determining the magnetic behavior in these phases. A quantitative description of the hybridization effects may be obtained via band structure calculations in the framework of the local spin density approximation. However, as shown in Ref. 16, a proper estimation of the strength of the f-s,p,d hybridization in series

TABLE IV. Hyperfine parameters of the ^{121}Sb Mössbauer spectra of the UTSb$_2$ (T=Cu, Ni, Pd, Ru) ternary antimonides and the related USb$_2$ compound. The isomer shifts (δ_{IS}) given are relative to the source at 4.2 K or 77 K (measurements performed in the paramagnetic state). W represents the linewidth of the Lorentzian line shape, H_{hf} is the hyperfine field, and $eV_{zz}Q$ stands for the effective quadrupole coupling constant. The labels (1) and (2) refer to the Sb1 and Sb2 atoms, respectively. The parameters fixed in the fitting procedure are marked by the symbol *.

Compound	T (K)	$H_{hf}^{(1)}$ (kOe)	$H_{hf}^{(2)}$ (kOe)	$eV_{zz}Q^{(1)}$ (mm/s)	$eV_{zz}Q^{(2)}$ (mm/s)	$\delta_{IS}^{(1)}$ (mm/s)	$\delta_{IS}^{(2)}$ (mm/s)	W (mm/s)
UCuSb$_2$	125			13.1(3)	−4.7(5)	−9.84(5)	−7.77(4)	2.79(9)
	4.2	115(1)	137(2)	13.1*	−4.7*	−9.65(3)	−7.80(3)	2.82(5)
UNiSb$_2$	186			12.8(6)	−6.5(6)	−9.9(1)	−7.93(8)	2.4(2)
	4.2	97(1)	106(1)	11.1(4)	−5.5(4)	−10.14(4)	−7.72(4)	2.40(6)
UPdSb$_2$	210			10.7(6)	−7.4(6)	−9.77(5)	−7.76(4)	2.5*
	4.2	120(1)	128(1)	9.9(3)	−7.8(3)	−10.30(3)	−7.48(3)	2.50(6)
URuSb$_2$	138			12.0(4)	−5.4(5)	−9.72(6)	−7.44(4)	2.5(2)
	4.2		44(1)	12.1(2)	−5.4*	−10.30(1)	−7.16(2)	2.7(3)
USb$_2$	4.2	122(1)	104(1)	9.9(4)	−6.0(3)	−9.68(4)	−8.99(4)	2.92(3)

of isostructural compounds may be obtained employing the method developed by Straub and Harrison.[17,18] This approach combines the linear muffin-tin orbital (LMTO) theory[19] with the transition-metal pseudopotential formalism[20] to yield the method for calculating two-center couplings between f orbitals of cerium or uranium and s, p, d orbitals of neighboring ligands. The input parameters of the model are the atomic radii of interacting atoms, r_l and $r_{l'}$, the distance between these atoms, d, the respective angular momenta, l and l' ($l,l'=0$, 1, 2, and 3 for s, p, d, and f orbitals, respectively), and the symmetry of the bond, m ($m=0$, 1, 2, and 3 for σ, π, δ, and φ bonds, respectively). The general hybridization matrix element has the form

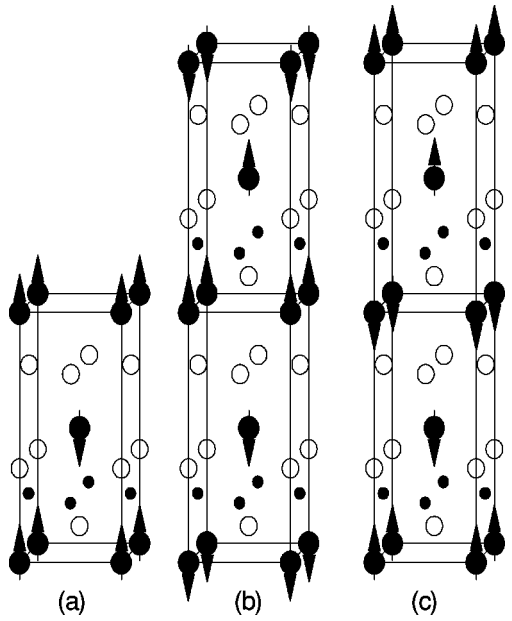

FIG. 8. Magnetic structures of antiferromagnetic UTX_2 compounds, crystallizing with the tetragonal HfCuSi$_2$-type unit cell. The arrows indicate the alignment of the uranium magnetic moments. Model (a) represents the structure adopted by UNiAs$_2$ and URuSb$_2$. Model (b) is appropriate for UPdAs$_2$. Model (c) shows the magnetic structure found for UNiSb$_2$ and UPdSb$_2$.

$$V_{ll'm}=\eta_{ll'm}\frac{\hbar^2}{m_e}\frac{(r_l^{2l-1}r_{l'}^{2l'-1})^{1/2}}{d^{l+l'+1}}, \tag{3}$$

where m_e is the free electron mass, and the coefficient $\eta_{ll'm}$ is given by

$$\eta_{ll'm}=\frac{(-1)^{l'+1}}{6\pi}\frac{(l+l')!(2l)!(2l')!}{2^{l+l'}l!l'!}(-1)^m \times\left[\frac{(2l+1)(2l'+1)}{(l+m)!(l-m)!(l'+m)!(l'-m)!}\right]^{1/2}. \tag{4}$$

The strength of f-l' hybridization can be estimated as follows:

$$V_{fl'}=\left[\sum_i\frac{n_i}{2l'+1}(V_{fl'\sigma}^2+2V_{fl'\pi}^2+2V_{fl'\delta}^2+2V_{fl'\varphi}^2)\right]^{1/2}, \tag{5}$$

where n_i is the number of neighbors with the angular momentum l' at a given distance d. According to Ref. 18, the second moment of the hybridized band

$$\langle(E_k-\varepsilon_f)^2\rangle=V_{fp}^2+V_{fd}^2+V_{ff}^2=V_{\text{total}}^2 \tag{6}$$

may be taken as a measure of the delocalization tendency of f electrons, while the square root of this quantity may be identified with the total covalent energy which contributes to the cohesion in a solid. Furthermore, Harrison and Straub[18] derived in their work a criterion for localization of magnetic moments: if V_{total} is smaller than $U\sin^2(Z_f\pi/14)$, where U stands for the Coulomb repulsion and Z_f is the number of f electrons, f-electron localization and magnetic ordering may be expected. In the case of uranium compounds the critical energy amounts to 680 and 1380 meV for f^2 and f^3 configuration, respectively. It is worthwhile noting at this point that in the case of well-localized systems, i.e., when the f-p,d hybridization does not result in creating bands, the matrix elements $V_{ll'm}$, given by Eq. (3), make the hybridization contribution to the ligand field and thus reappear in single-ion anisotropy.

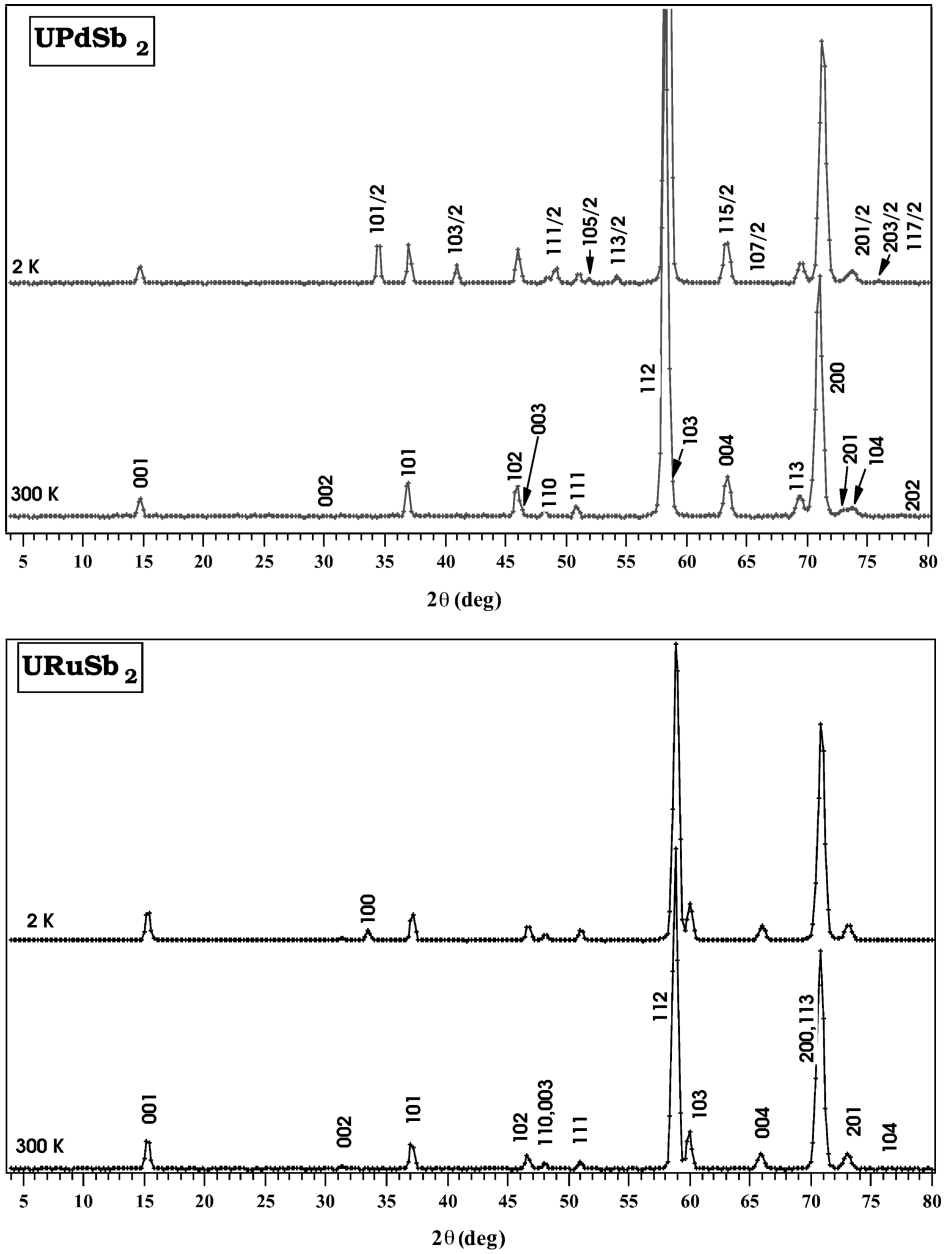

FIG. 9. Neutron diffraction patterns of $UPdSb_2$ and $URuSb_2$ at 300 K and 2 K.

In the following the above described approach was applied on UTX_2 compounds. The calculations have been performed for all the phases for which the precise structural data are known: $UCuP_2$,[21] $UCuAs_2$,[1] $UNiAs_2$,[14] $UCoAs_2$,[22] $UPdAs_2$,[13] and studied here, $URuSb_2$ and $UPdSb_2$ (Tables V and VI). Moreover, for comparison, the parent compounds UP_2, UAs_2, and USb_2 (Ref. 23) have also been taken into consideration. The atomic radii of the respective atoms were taken from Refs. 17 and 18. The results of the calculations are collected in Table VII.

As is apparent from this table, a direct mutual overlap of $5f$ orbitals of uranium is almost negligible in all the compounds considered (V_{ff} is less than 0.5% of V_{total}). This finding is in accord with the Hill criterion for the f-electron localization because the shortest U-U distances are here always much larger than 3.4 Å. The total hybridization energy in UTX_2 pnictides is given mainly by the f-p contribution which amounts to above 90% of V_{total} in the phosphide and all the arsenides, and 70–80 % of V_{total} in the case of two antimonides. Yet, it is worth noting that the magnitude of V_{fp} does not change much within a given series of pnictides being close to that value derived for the respective parent UX_2 compound (except for UP_2). This feature suggests that the magnetic properties which are common for all these phases, e.g., strong ferromagnetic coupling of the magnetic moments within uranium atom layers and huge magnetic anisotropy (for discussion see, for example, Ref. 24), may be caused by the f-p mixing, as it is the case in cerium and uranium monopnictides and monochalcogenides.[25]

In turn, the f-d hybridization in UTX_2 compounds is rather moderate, V_{fd} being only 3% of V_{total} in $UCuP_2$ and 3–11 % of V_{total} in the arsenides. Only in the case of $URuSb_2$ and $UPdSb_2$ does V_{fd} make a big contribution to V_{total} (28% and 16%, respectively). Yet, in all the compounds considered the strength of f-d hybridization varies significantly upon exchange of T component. For example, within the group of ternary uranium arsenides containing a $3d$-electron transition metal, V_{fd} increases by 30% when Cu is replaced by Ni, and

TABLE V. Observed and calculated intensities at 300 and 2 K and refined parameters for $UPdSb_2$.

	300 K		2 K	
hkl	F_o^2	F_c^2	F_o^2	F_c^2
001	9	13	41	45
002	<5	<5	<5	<5
$10\frac{1}{2}$			503	499
101	133	128	401	416
$10\frac{3}{2}$			263	276
102, 003	186	193	721	730
110	38	42	131	124
$11\frac{1}{2}$			428	417
111	73	66	185	197
$10\frac{5}{2}$			92	108
$11\frac{3}{2}$			267	260
112, 103	4122	4274	14009	14216
004, $11\frac{5}{2}$	472	483	1662	1685
$10\frac{7}{2}$			63	67
113	375	359	1001	1013
200	4222	4301	12439	12588
201	107	114		
$20\frac{1}{2}$			701	731
104	122	117		
$20\frac{3}{2}$, $11\frac{7}{2}$			433	466
a (Å)	4.325(1)		4.316(1)	
c (Å)	9.552(2)		9.545(2)	
f_{cor}	1.17(1)		1.18(1)	
z_U	0.252(1)		0.252(1)	
z_{Sb2}	0.674(1)		0.677(1)	
μ_0 (μ_B)			2.15(10)	
R(%)	2.3		1.6	

TABLE VI. Observed and calculated neutron diffraction intensities at 300 and 2 K and refined parameters for $URuSb_2$.

	300 K		2 K	
hkl	F_o^2	F_c^2	F_o^2	F_c^2
001	42	46	142	148
002	<5	<5	<5	<5
100			198	192
101	231	211	1273	1293
102	143	152	432	455
110, 003	184	180	792	829
111	87	94	928	952
112	6107	6215	20628	20971
103	725	772	3122	3143
004	378	406	1393	1419
200, 113	4112	4141	13564	13884
201	498	477	1802	1764
104	<5	<5	25	22
a (Å)	4.335(1)		4.330(1)	
c (Å)	9.230(2)		9.221(2)	
f_{cor}	1.27(1)		1.28(1)	
z_U	0.263(1)		0.264(1)	
z_{Sb2}	0.652(1)		0.651(1)	
μ_0 (μ_B)			1.20(9)	
R(%)	1.5		1.8	

as much as by 43% when Cu is substituted by Co. Similarly, in the group of ternary uranium antimonides containing a $4d$-electron transition metal, V_{fd} increases by 42% when Pd is substituted by Ru. As seen from Table VII, the changes in the magnitude of the f-d hybridization in UTX_2 pnictides do not yield any appreciable weakening in the $5f$-electron localization because V_{total} is always much larger than the critical value of 680 meV (appropriate for compounds based on U^{4+} ions). However, as noted above, the change in V_{fd} results in different types of the magnetic coupling between adjacent uranium atom layers occurring. Therefore it seems likely that just the f-d interactions govern the overall magnetic behavior of UTX_2 compounds, i.e., the strength of the f-d hybridization may decide if a given compound is ferromagnetic or antiferromagnetic and what the type of its magnetic structure is.

V. SUMMARY

For many years the problem of localization of f electrons in a solid has been the central point of actinide research. It is commonly believed that the degree of $5f$-electron localization is mainly determined by the interactions of $5f$-electron states with s-, p-, and d-electronic states of surrounding atoms. The way to study the hybridization effects is such a modification of the neighborhood of a given f-electron atom in which only a selected factor (e.g., the coordination number, the spatial arrangement of ligands, their electronic character, etc.) is being changed in a systematic manner, while keeping all the other factors unaltered. In practice, this task is usually realized by detailed investigations carried out on long series of isostructural compounds. The best examples here are the results obtained on well-known numerous families of UT_2M_2 and UTM (M=Si, Ge) intermetallics (for a review see Ref. 26).

The group of UTX_2 pnictides is another example of such a series of ternary uranium phases, and the compounds re-

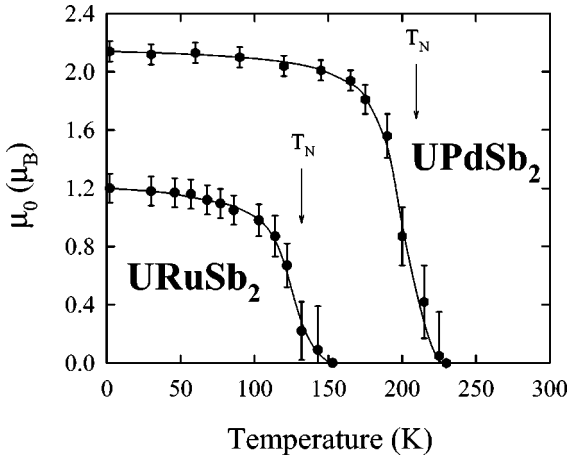

FIG. 10. Temperature dependence of the uranium magnetic moment in $UPdSb_2$ and $URuSb_2$.

TABLE VII. Contributions of the f-$f(V_{ff})$, f-$d(V_{fd})$, and f-$p(V_{fp})$ hybridization to the total covalent energy (V_{total}) in UTX_2 and UX_2 compounds.

Compound	V_{ff} (meV)	V_{fd} (meV)	V_{fp} (meV)	V_{total} (meV)
UP_2	90		1698	1700
$UCuP_2$	91	195	1173	1193
UAs_2	69		1137	1139
$UCuAs_2$	70	190	1006	1026
$UNiAs_2$	70	245	1021	1052
$UCoAs_2$	68	271	999	1037
$UPdAs_2$	65	355	1028	1088
USb_2	41		882	883
$URuSb_2$	36	493	793	934
$UPdSb_2$	37	347	810	882

ported here with $X=$Sb considerably enlarge the number of family members. The antimonides with $T=$Co, Cu, Ag, and Au have been found to order ferromagnetically, while those with $T=$Ni, Ru, and Pd to order antiferromagnetically at low temperatures. The magnetic structures of the latter compounds have been determined by combined studies of Mössbauer effect and powder neutron diffraction. Most of these $UTSb_2$ phases exhibit an interplay of crystal-field and Kondo-like effects which results in considerable reductions of uranium magnetic moments.

The magnetic behavior of the antimonides studied here, as well as their phosphide and arsenide relatives, can be attributed to superexchange and RKKY exchange interactions, modified by f-p and f-d hybridization. In particular, the strong anisotropy, characteristic of all these compounds, is probably due to pronounced f-p mixing, whereas the type of magnetic ordering is presumably correlated to the magnitude of f-d overlap. The results of the semiquantitative analysis of the hybridization effects in UTX_2 compounds, performed employing the method proposed by Harrison and Straub, entirely support the above hypothesis. However, a more advanced theoretical study is needed to get complete and reliable information about the electronic structure of these materials. This requirement is the more important as some further experimental attempts to synthesize and physically characterize several brand new representatives of the UTX_2 series are now underway.

ACKNOWLEDGMENTS

Part of this work was sponsored by the Polish Committee for Scientific Research within the Project No. 2 P03B 147 10. R.K. gratefully acknowledges CEA-Grenoble for its hospitality and financial support.

*Author to whom correspondence should be addressed.
†Permanent address: Institute of Nuclear Physics, Cracow, Poland.

[1] J. Stepień-Damm, D. Kaczorowski, and R. Troć, J. Less-Common Met. **132**, 15 (1987).
[2] L. S. Andrukhiv, L. A. Lysenko, Ya. P. Yarmolyuk, and E. I. Gladyshevskii, Dopov. Akad. Nauk. Ukr. RSR, Ser. A: Fiz.-Mat. Tekh. Nauki **XX**, 645 (1975).
[3] M. Brylak, M. H. Möller, and W. Jeitschko, J. Solid State Chem. **115**, 305 (1995).
[4] D. Kaczorowski, J. Alloys Compd. **186**, 333 (1992).
[5] R. Welter, G. Venturini, and B. Malaman, J. Alloys Compd. **189**, 49 (1992).
[6] C. G. Shull and Y. Yamada, J. Phys. Soc. Jpn. **22**, 1210 (1962).
[7] P. Wolfers, J. Appl. Crystallogr. **23**, 554 (1990).
[8] J. Rossat-Mignod, G. H. Lander, and P. Burlet, in *Handbook on the Physics and Chemistry of the Actinides*, edited by A. J. Freeman and G. H. Lander (North-Holland, Amsterdam, 1984), Vol. 1.
[9] M. Maurer, M. C. Cadeville, and J. P. Sanchez, Philos. Mag. A **38**, 739 (1978).
[10] J. P. Sanchez, J. C. Spirlet, J. Rebizant, and O. Vogt, J. Magn. Magn. Mater. **63-64**, 139 (1987).
[11] J. Leciejewicz, R. Troć, A. Murasik, and A. Zygmunt, Phys. Status Solidi **22**, 517 (1967).
[12] J. Przystawa, Phys. Status Solidi **30**, K115 (1968).
[13] A. Murasik, P. Fischer, and D. Kaczorowski, J. Phys.: Condens. Matter **2**, 3967 (1990).
[14] P. Fischer, A. Murasik, D. Kaczorowski, and R. Troć, Physica B **156&157**, 829 (1989).
[15] D. D. Koelling, B. D. Dunlap, and G. W. Crabtree, Phys. Rev. B **31**, 4966 (1985).
[16] T. Endstra, G. J. Nieuwenhuys, and J. A. Mydosh, Phys. Rev. B **48**, 9595 (1993).
[17] G. K. Straub and W. A. Harrison, Phys. Rev. B **31**, 7668 (1985).
[18] W. A. Harrison and G. K. Straub, Phys. Rev. B **36**, 2695 (1987).
[19] O. K. Andersen, Phys. Rev. B **12**, 3060 (1975).
[20] W. A. Harrison, Phys. Rev. **181**, 1036 (1969).
[21] H. Noël, Z. Żolnierek, D. Kaczorowski, and R. Troć, J. Less-Common Met. **132**, 327 (1987).
[22] D. Kaczorowski, M. Potel, and H. Noël (unpublished).
[23] J. M. Fournier and R. Troć, in *Handbook on the Physics and Chemistry of the Actinides*, edited by A. J. Freeman and G. H. Lander (North-Holland, Amsterdam, 1985), Vol. 2.
[24] D. Kaczorowski, R. Troć, and H. Noël, J. Phys.: Condens. Matter **3**, 4959 (1991).
[25] K. Takegahara, A. Takahashi, A. Yanase, and T. Kasuya, J. Phys. C **14**, 737 (1981); Solid State Commun. **39**, 857 (1981).
[26] V. Sechovsky and L. Havela, in *Ferromagnetic Materials*, edited by E. P. Wohlfarth and K. H. Buschow (North-Holland, Amsterdam, 1988), Vol. 4, p. 309.